

Robustness of a flux-intensifying permanent magnet-assisted synchronous reluctance machine focusing on shifted surface-inset ferrite magnets

Mihály Katona*, Tamás Orosz

Department of Power Electronics and Electric Drives, Széchenyi István University, Egyetem tér 1., Győr, 9026, Hungary



HIGHLIGHTS

- Remanufacturing an existing PMSM servo machine to a flux-intensifying permanent magnet-assisted synchronous reluctance machine for a different application.
- Robustness is assessed using the Taguchi method and validated by full factorial calculations.
- The resulting machine design of the proposed procedure is less sensitive to magnet shifting during assembly than part manufacturing.
- Using the magnet shifting procedure, a 31.25 % reduction in magnet volume still achieves the same torque output.
- Micromobility application without reverse motoring enables asymmetric rotor structure such as shifted magnets.

ARTICLE INFO

Keywords:
 Electrical machines
 Optimisation
 Finite element method
 Robust design
 Circular economy
 Remanufacturing
 Taguchi method

ABSTRACT

Flux-intensifying permanent magnet-assisted synchronous reluctance machines use relatively small amounts of non-rare earth permanent magnets, making them viable alternatives for remanufacturing older machines, aligning with EU directives and circular economy principles. The asymmetric rotor topology is particularly suited for micromobility applications, which benefit from shifting inset magnets, as reverse motoring is rarely required. However, this design could be more sensitive to manufacturing and positioning errors of the magnets. To investigate the effects of the uncertainties of the shifted surface inset magnets, first, an optimal topology is selected based on average torque, torque ripple, and cogging torque using the NSGA-II optimisation method. The effects of the magnet shifting and its robustness are analysed using the Taguchi and ANOVA methods, validated by Full Factorial calculations. Results indicate a 31.25 % reduction in permanent magnet volume without compromising torque output with magnet shifting. The machine's average and cogging torque remain within a 5 % robustness threshold for a ± 0.06 mm discrete manufacturing tolerance. Torque ripple may exceed this limit up to 14.77 %. However, the likelihood of exceeding the threshold is only 12.10 %. The reduced magnet volume and maintained performance make this topology a promising option for remanufactured machines in micromobility applications, supporting circular economy goals.

1. Introduction

Remanufacturing electric machines is a complex method for extending their lifespan. This process belongs to the main circular economy concepts and involves preferably nondestructive disassembly, refurbishing, and reusing the intact components. It often includes redesigning the rotor or the winding to achieve higher efficiency or accommodate a different intended use than the original design. The goal of remanufacturing is to ensure that the remanufactured product satisfies the quality of a new product, in contrast to simple refurbishment [1,2].

Although there are many definitions of remanufacturing [3,4], this paper will adhere to the aforementioned definition, as it aligns with similar definitions in relevant studies [5,6].

Many papers have published case studies and examined the economic and technological aspects of different industrial applications of remanufacturing. In the case of an industrial 110 kW asynchronous machine, it has been demonstrated that converting an end-of-life (EoL) asynchronous machine into a permanent magnet synchronous machine (PMSM) can increase the machine's efficiency from approximately 91 % to 94.6 % by changing the rotor structure. This 3.6 % improvement

* Corresponding author.

Email address: katona.mihaly@sze.hu (M. Katona).



Fig. 1. The investigated EoL electric machine and its reusable parts.

Table 1
Main parameters of the EoL electric machine as a basis for redesign.

Parameter	Value	Unit
Stator diameter	86.5	mm
Rotor diameter	44	mm
Number of slots	12	–
Number of poles	8	–
Stack length	40	mm
Air gap	1	mm
RMS current	103.19	A
DC bus voltage	48	V

translates to an annual electricity savings of about \$18,000, based on an electricity cost of 9 cents per kWh. In contrast, the estimated material cost of remanufacturing is around \$18,000 [6]. Considering that labor costs and energy consumption during the remanufacturing process remain the same, the break-even point is less than three years, which is advantageous in an industrial setting.

Remanufacturing asynchronous machines into PMSMs also significantly reduces environmental impact, particularly in scenarios where the rotor core is remanufactured and the bearings are replaced. At the same time, other components can be reused instead of manufacturing a new PMSM [7]. This paper presents a similar process. The investigated electric machine is an EoL PMSM, in which the intact housing, shaft, and stator are reused. The bearings are replaced, while the windings and rotor are redesigned and replaced, following the inspection processes described in [5,8]. The investigated electric machine is shown in Fig. 1, and the main geometrical parameters are summarized in Table 1.

The recycling rate of the world for materials based on rare earth elements (REE), mostly permanent magnets (PMs) in electric motors, is less than 3 %. One possible reason is the disassembly difficulties of interior PM machines where the PMs are glued into the rotor stacks [9,10]. In a circular economy, an electric machine should be sustainable by design, which means facilitating the machine's ability to reuse, recycle, refurbish, and remanufacture—during the early design—at the end of its lifetime. Inset PMs in the circumference of the rotor could be a solution to facilitate the complex disassembly of the machines. Other factors make remanufacturing and the implementation of the principles of circular economy complicated as well. The lack of information on returned products and their variability, the cost vs. return on investment, and the lack of methodologies to decide the EoL scenario for electric machines are not within the scope of this research [9,11]. On the other hand, electric machines have a high potential for remanufacturing [10].

According to the end-of-life vehicle regulations of the European Union [12], the directive requires that 85 % of a vehicle be repurposed or recycled by weight, encouraging the remanufacturing of the components and the recycling of PM. The efficient recovery and recycling of critical elements, such as REEs from electrical machine PMs, is important for countries without rare earth deposits, as they are susceptible to market instabilities in the supply of these materials. REEs make up an

estimated 40–60 % of the active material cost of current electric machine designs. In contrast, remanufactured parts generally cost around 50–75 % of the price of new components [10]. In this paper, a ferrite magnet-based design was examined because this material is more accessible and more easily reused than the neodymium magnets and because it facilitates sustainability aspects. The PM used for the simulation is a Y30 ferrite magnet, and the stator steel is based on the laboratory measurements of the remanufactured EoL electric machine's stator. The rotor material is based on the laboratory measurement of Fe-6.5 wt%Si alloy optimised for laser sintering [13]. The measurement method is described in [8]. The model, algorithm and results are stored in the 'synrm' branch of <https://github.com/tamasorosz/py2femm>.

This paper deals with the redesign possibilities of a mass-manufactured servo PMSM rotor into a rare-earth magnet-free solution within remanufacturing. The remanufactured machine is a flux-intensifying permanent magnet-assisted synchronous reluctance machine (FI-PMASynRM) type for a new micromobility application. Four possible rotor geometries are optimised, which differ in the direction of magnet shifting and the presence of air barriers next to the magnets. To determine the sensitivity of the objective function, which includes the average torque, the torque ripple, and the cogging torque, to the design variables, the Taguchi and Analysis of Variance (ANOVA) methods are used following an NSGA-II optimisation process. The optimal design is selected using the Technique for Order Preference by Similarity to Ideal Solution (TOPSIS) and Stable Preference Ordering Towards Ideal Solution (SPOTIS) methods.

In a FI-PMASynRM, the inset magnets are embedded into the circumference of the rotor, which could ease the disassembly process, facilitating disassembly and, thus, reuse of the magnets or recycling of the machine. However, the hypothesis of this research is that the torque output, torque ripple, and cogging torque of the redesigned machine are more sensitive to changes in the main geometrical parameters of the rotor sheets within the manufacturing tolerance range than to the shifted magnet positioning. This implies that the robustness of the machine is more dependent on the manufacturable parameters than on the assembly process, where the manufacturing is more precisely controllable than the assembly process.

The selected design is investigated in terms of robustness within the manufacturing tolerance range to support the hypothesis using Taguchi method, which is compared to the Full Factorial solution to determine the Taguchi method's performance in terms of extreme value approximation. The effects of magnet shifting and the width of the air barrier affected by manufacturing uncertainties are calculated using ANOVA on the Full Factorial solution.

Section 2 covers the methodology, including the theoretical overview of the FI-PMASynRM, the shifting of inset magnets, the investigated design cases, sensitivity analysis, optimisation, multi-criteria decision-making, and robust design analysis. **Section 3** summarises the results which the conclusion follows.

2. Methodology

2.1. Theoretical overview of flux-intensifying permanent magnet-assisted synchronous reluctance machines

The FI-PMASynRM was proposed to reduce PM demagnetisation while enhancing the torque output of a synchronous reluctance machine with a limited amount of PMs. The flux-intensifying feature comes from adding the PM to the direct (*d*) axis of the rotor instead of the quadrature (*q*) axis, thus complementing the *d*-axis flux linkage produced by the *d*-axis current [14]. In a permanent magnet-assisted synchronous reluctance machine (PMASynRM) without a flux-intensifying feature, the PMs are added to the *q*-axis, reducing the flux linkage produced by the *q*-axis current [15]. Following the definitions of [14], the rotor of the investigated FI-PMASynRM consists of a Magnet Flux Barrier (MFB) that contains the inset PM, the Interior Flux Barrier (IFB) and the Cut-off Flux Barrier (CFB) shown in Fig. 2. The differences between a PMASynRM

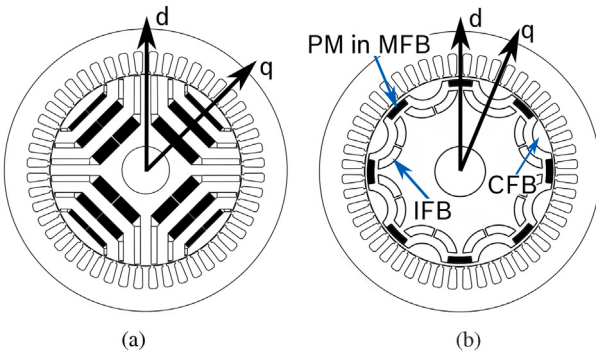


Fig. 2. Rotor topology for (a) PMASynRM [1,16] and (b) the investigated FI-PMASynRM based on [14,17-19] where PM: permanent magnet, MFB: magnet flux barrier, IFB: internal flux barrier and CFB: cut-off flux barrier.

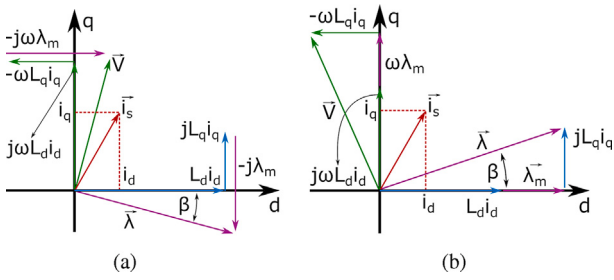


Fig. 3. Phasor diagram of (a) PMASynRM [15] and (b) FI-PMASynRM [14].

and an FI-PMASynRM are represented on a phasor diagram in Fig. 3. The torque equations are presented in (1) and (2) for PMASynRM and FI-PMASynRM in order [14,15].

$$T_{PMASynRM} = \frac{3}{2} p((L_d - L_q)i_d i_q - \lambda_m i_d) \quad (1)$$

$$T_{FI-PMASynRM} = \frac{3}{2} p(\lambda_m i_q + (L_d - L_q)i_d i_q) \quad (2)$$

where:

- p: number of pole pairs [-]
- L_d : direct axis inductance [ht]
- L_q : quadrature axis inductance [ht]
- i_d : direct axis current [A]
- i_q : quadrature axis current [A]
- λ_m : PM flux linkage [Wb]

One property of the FI-PMASynRM that distinguishes it from Flux-Intensifying Interior Permanent Magnet (FI-IPM) synchronous machines is the dominant reluctance torque in contrast to magnetic torque [17] shown in Fig. 4a. During the applied optimisation procedure, any optimal machine with higher reluctance torque than magnetic torque is classified as a FI-PMASynRM presented in Fig. 4b. The method to divide the magnetic and reluctance torque in the case of FI-PMASynRM was presented in [17].

The influence of the CFB, IFB, MFB and PM dimensions has already been investigated on the average torque and torque ripple, and the displacement of the CFB, MFB and PM as well [14,18]. The results show that the depth of the CFB does not significantly influence the average torque, but the torque ripple depends on it. The IFB shows similar effects, but its thickness considerably increases the average torque. The displacement of the CFB increases the torque ripple. Finally, the shift of PMs with MFB can result in a considerable reduction in torque ripple [14]. However, the presented studies focus on the influence of the different parts individually, without considering the effects on each other.

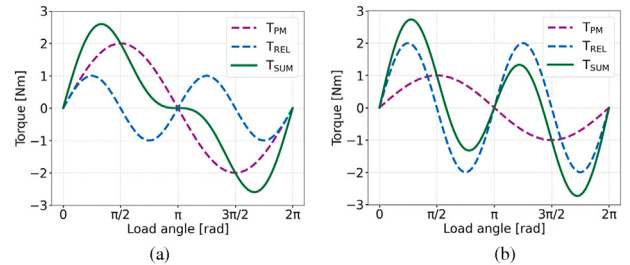


Fig. 4. Torque components for (a) FI-IPM and (b) FI-PMASynRM where T_{PM} denotes magnetic torque and T_{REL} marks reluctance torque and T_{SUM} the resulting torque [14].

Furthermore, adding PMs to the rotor introduces cogging torque which this paper considers as well. The NVH (noise, vibration, and harshness) factors are an important aspect of the automotive industry even in micromobility to increase driver comfort and extend the lifespan of the product. It is important to consider motor design parameters to minimise torque ripple and the cogging torque as well [20].

The FI-PMASynRM can be separated into two subsequent models: one with solely reluctance torque without PMs, basically a SynRM and one with only the PMs and no FBs. Comparison of the ratio of direct and quadrature inductances (L_d/L_q)—called saliency ratio—of the different models shows that by increasing the armature current, the direct inductance of the SynRM decreases more significantly than the FI-PMASynRM maintaining a higher saliency ratio over high currents. Furthermore, the demagnetisation of the inset PMs comes at higher currents in the case of FI-PMASynRM.

The equivalent magnetic circuit model for this machine type was also created to calculate the direct and quadrature inductances, considering saturation analytically. The results show a 3–6 % difference from the Finite Element Method (FEM) calculations and can be used to simplify the motor design process [19]; however, in the present investigation, FEM analysis is presented. The field weakening capabilities were investigated considering the PM dimension and the armature current simultaneously. Even though a larger PM span produces higher PM flux, thus reducing the required armature current for the desired output to improve the constant power-speed range of the machine, the larger PM span is not necessarily beneficial. Extending the PM span increases the magnet volume faster than expanding the constant power-speed range. Furthermore, it significantly adds to manufacturing costs. The cited study highlights the importance of the PM dimension but assumes a predetermined flux barrier (FB) topology [18].

2.2. Magnet shifting and the design cases

In the case of a motor model where there are only inset PMs on the circumference of the rotor without flux barriers, called an inset Surface-mounted Permanent Magnet Synchronous Machine (inset SPMSM)—shown in Fig. 5a—shifting means a change in the magnetic pole between the PMs placed in every pole of the machine, which offers a significant reduction in torque ripple [21]. In the case of FI-PMASynRM, magnet shifting means an offset from the center line of the machine's pole.

Based on [21], counter-clockwise magnet shifts were adopted in this paper, as well, because of the symmetry of forward rotation with counter-clockwise shifts to backward rotation with clockwise shifts. Air barriers next to the magnet—meaning an extension of the MFB wider than the PM itself—can reduce torque ripple while enhancing the use of the reluctance torque as well [22]. If “all Repeating Units (RU) produce torque waveforms with the same amplitudes and the same phases including total torque, reluctance torque, and cogging torque”, then one pole-pair as an RU is optimal for reducing cogging torque [21]. This paper compares one pole as RU where all PMs are counter-clockwise

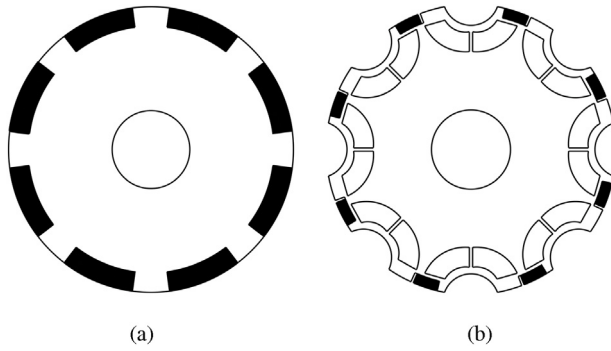


Fig. 5. Comparison of (a) inset SPMMSM [21] and (b) FI-PMASynRM [14].

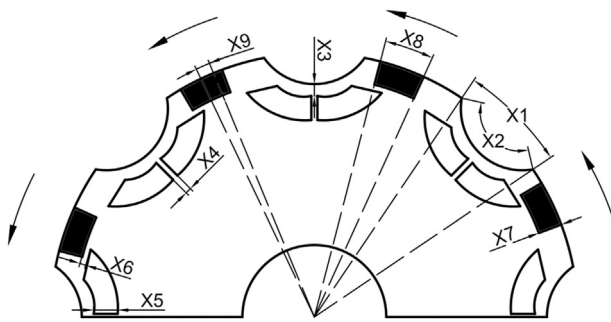


Fig. 6. Design variables for Case A1 in which all magnets are shifted in the same direction in every pole. The design variables are summarised in Table 2.

Table 2
Design variables and their ranges for Cases A1 and A2.

Variable	Meaning	Range	Unit
X_1	Opening angle of CFB	15–25	deg
X_2	Included angle of CFB	100–150	deg
X_3	Distance between the CFB and IFB	1–4	mm
X_4	Width of the rib at IFB	0.5	mm
X_5	Height of IFB	1–4	mm
X_6	Distance between the PM and IFB	0.5–1	mm
X_7	Height of the PM	1.5	mm
X_8	Width of the PM	10–15	deg
X_9	Shift of the PM	0–16	deg

shifted (Cases A1 and B1) and two pole pairs as one RU where in two adjacent poles, one PM is shifted counter-clockwise and the other clockwise (Cases A2 and B2). The difference between Cases A and B is the introduction of air barriers. The utilisation of RUs reflects the symmetry of the motor structure. An RU represents a collection of poles that generate torques with consistent waveforms and phases, making it possible to utilise the machine's periodic and antiperiodic symmetry.

2.2.1. Case A1: one pole as repeating unit without air barriers

In Case A1, one pole as an RU is chosen, meaning one pole can represent the machine using antiperiodic boundary conditions as every magnet in every pole is shifted in the same counter-clockwise direction, also known as unidirectional shifting [22]. The direction of the magnet's shift and the design variables are shown in Fig. 6, and the latter is also summarised in Table 2.

2.2.2. Case A2: two poles as one repeating unit without air barriers

Case A2 is similar to Case A1 regarding design variables presented in Table 2. The difference is the bidirectional magnet shifting [22] and the two poles as RU design, meaning that in every two adjacent poles,

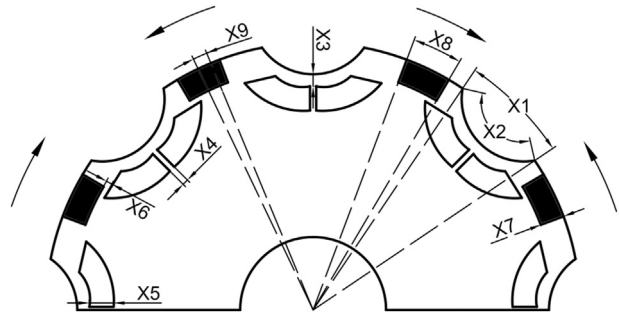


Fig. 7. Design variables for Case A2 in which the magnets are shifted in the opposite direction for every pole pair. The design variables are summarised in Table 2.

one PM is shifted counter-clockwise and the other is shifted clockwise, as shown in Fig. 7.

2.2.3. Case B1: one pole as repeating unit with air barriers

Case B1 is similar to Case A1 regarding the shifting method and repeating units. The difference is the introduction of the air barriers between the magnet and the rotor sheets meaning an extension of the MFB wider than the PM itself presented in Fig. 8. The design variables are summarised in Table 3.

2.2.4. Case B2: two poles as one repeating unit with air barriers

By the shifting method and repeating units, Case B2 is similar to Case A2. The difference is the introduction of the air barriers. The design variables are presented in Fig. 9. The design variables are summarised in Table 3.

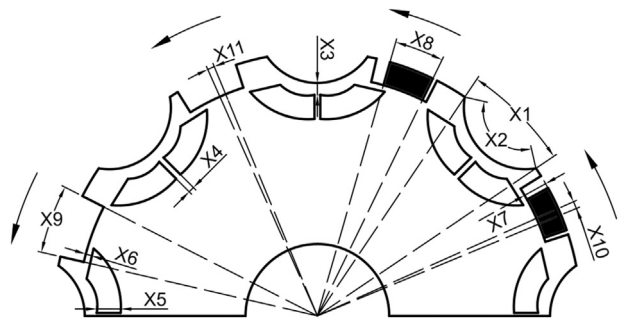


Fig. 8. Design variables for Case B1, in which all magnets and MFBs are shifted in the same direction in every pole. The magnets on the left side poles are deliberately omitted from the figure to emphasise the MFBs, but there are magnets in the simulations. The design variables are summarised in Table 3.

Table 3
Design variables and their ranges for Cases B1 and B2.

Variable	Meaning	Range	Unit
X_1	Opening angle of CFB	15–25	deg
X_2	Included angle of CFB	100–150	deg
X_3	Distance between the CFB and IFB	1–4	mm
X_4	Width of the rib at IFB	0.5	mm
X_5	Height of IFB	1–4	mm
X_6	Distance between the PM and IFB	0.5–1	mm
X_7	Height of the PM	1.5	mm
X_8	Width of the PM	10–15	deg
X_9	Width of MFB	10–18	deg
X_{10}	Shifting angle of PM	0–16	deg
X_{11}	Shifting angle of MFB	0–16	deg

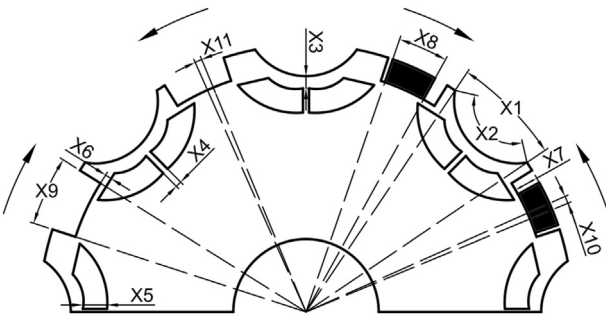


Fig. 9. Design variables for Case B2 in which the magnets and MFBs are shifted oppositely for every pole pair. The magnets on the left side poles are deliberately omitted from the figure to emphasize the MFBs, but there are magnets in the simulations. The design variables are summarised in Table 3.

Table 4
The first five models are defined by the design parameters for Case A1.

Exp.	X1	X2	X3	...	X8	X9	Navg	Nrip	Ncog
1	15.0	10.0	1.0	...	10.0	0.0	0.00	0.08	0.20
2	15.0	10.0	1.0	...	12.5	8.0	0.22	0.81	0.64
3	15.0	10.0	1.0	...	15.0	16.0	0.22	0.94	0.78
4	15.0	12.5	2.5	...	12.5	8.0	0.31	0.37	0.27
5	15.0	12.5	2.5	...	15.0	16.0	0.39	0.51	0.50
:	:	:	:	:	:	:	:	:	:

2.3. Sensitivity analysis, optimisation and multi-criteria decision making

2.3.1. Sensitivity analysis

Sensitivity analysis is meant to quantify the relative effect one design parameter or the combined effect of several parameters has on the objective functions used to determine the design variables required to be included in the optimisation or the robustness computation. There are different methods to approach the sensitivity analysis, for example, the H index and the level sensitivity analysis [23]. Another possibility is to use the Taguchi method and analysis of variance (ANOVA) [24]. In this paper the Taguchi method was utilised with an orthogonal matrix of L27 [25] with 13 factors and three levels to sample the design space combined with ANOVA.

The first five models defined by the design parameters and the normalised results of the objective functions—the average torque (Navg), the torque ripple (Nrip) and the cogging torque (Ncog)—are presented in Table 4 as an orthogonal matrix. The results of the objective functions are normalised to the scale of 0 to 1 to serve as a basis for ANOVA within a similar range for comparison.

The ANOVA method defines a parameter that quantifies the variation in groups evaluated through a weighted sum of squared deviations of the sample means from the overall mean, with each deviation weighted by its respective sample size called the sum of squares between groups (SSG) [26]. The SSG value for each factor is the sum of the SSG of each level in the respective factor and is calculated with Eq. (3) where $i \in [avg, rip, cog]$ denotes the different objective functions, $j \in [X1 \dots Xn]$ representing the investigated design parameter, $k \in [1, 2, 3]$ defining the level and \bar{N} is the mean value of the objective functions for the respective experiments grouped by the levels of a given design parameter.

$$SSG_{i,j} = \sum_{k=1}^3 n_{i,j,k} (\bar{N}_{i,j,k} - \bar{N}_{i,k})^2 \quad (3)$$

The higher the SSG value, the higher the design variable's effect on the objective function is relative to the other design parameters. The results of the sensitivity analysis are summarised in Section 3.1.

2.3.2. Optimisation

The Non-dominated Sorting Genetic Algorithm II (NSGA-II) is an effective multi-objective optimisation algorithm in electric machine design. NSGA-II can handle multiple conflicting objectives simultaneously, which is crucial in electric machine design where trade-offs between the maximisation of the average torque output and the minimisation of torque ripple and cogging torque are common. The algorithm generates a set of Pareto-optimal solutions, allowing one to choose from a range of optimal designs using multi-criteria decision-making algorithms. It is capable of handling large-scale optimisation problems efficiently, making it suitable for complex electric machine designs. The algorithm has been proven to be appropriate for multi-objective optimisation of a bearingless PMA-SynRM [27], PMA-SynRM with field line shaped barriers [28] or implementation of the cost as an objective function next to the electromagnetic properties in the case of a ferrite PMA-SynRM [29]. In this paper, the conflicting objectives are the maximisation of the average torque (f_{avg}) against the minimisation of the torque ripple (f_{rip}) and cogging torque (f_{cog}). The initial population of the optimisation process started with 100 models, with 50 models in each following generation where the termination criterion was 350 maximal generations or convergence based on the multi-objective termination criterion of *pymoo* package [30]. The framework for the discrete variable optimisation is established in *py2femm* [31], a Python programming language-based interface for Finite Element Method Magnetics solver [32].

$$\max: f_{avg}(X_1 \dots X_n)$$

$$\min: f_{rip}(X_1 \dots X_n)$$

$$\min: f_{cog}(X_1 \dots X_n)$$

where $X_1 \dots X_n$ are in the range provided in Tables 2 and 3. The goal for the objective functions is $f_{avg} \geq 1400$ mNm, $f_{rip} \leq 20\%$ and $f_{cog} \leq 22$ mNm for micromobility applications as electric bikes [33] or scooters [34] which are also based on the initial capability of the EoL servo PMSM.

2.3.3. Multi-criteria decision making

The Order Preference by Similarity to an Ideal Solution (TOPSIS) method efficiently selects the optimal design for PMASynRM [35]. Stable Preference Ordering Towards Ideal Solution (SPOTIS) [36] has also been applied for its lower sensitivity to small changes in data or criteria weights and its resilience to rank reversal. The two methods were utilised simultaneously to establish a reliable basis for choosing the optimal model on the feasible part of the Pareto front. For calculating the criteria weights, the entropy method can amplify the impact of attributes with a high diversity and reduce the influence of characteristics with low diversity in decision-making or evaluation [37]. The calculated weights for the entropy method are [$w_{avg} = 0.219$; $w_{rip} = 0.668$; $w_{cog} = 0.113$] indicating the highest variability in the torque ripple and the least in cogging torque. As all the models have lower cogging torque amplitude than the objective the weight of cogging torque is neglected.

2.4. Robust design analysis

Another aspect of the magnet shifting is the sensitivity of the machine's output, such as the average torque, the torque ripple, and the cogging torque, especially if there is a gap between the PM edges and the edges of the MFB as it is highly dependent on the assembly process which tends to be less precise than part manufacturing. A crucial aspect of a redesign process is that the redesigned part—in this case, the rotor—should be robust, meaning the change in the objective function (Δf) is negligible under the uncertainty due to changes in design parameter (Δx). Furthermore, the optimum values of the global optimum (f_{glob}) and robust (f_{rob}) optimum values are within the feasibility threshold (f_{th}) defined at the beginning of the redesign process. The global optimum is not necessarily robust but ensures manufacturing reliability [38,39]. A representation of robustness is shown in Fig. 10.

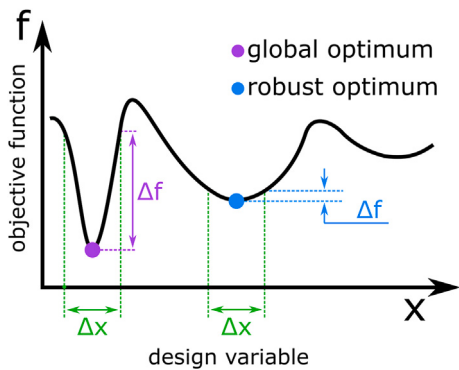


Fig. 10. Local and robust optima [38].

Optimisation can generally prioritise designs that demonstrate high performance ratings but lack robustness in the face of unavoidable tolerances and uncertainties associated with manufacturing and operation. The robust design optimisation has been divided into two subcategories: one focusing on the analysis of a single or a few optimum designs, and the other addressing the incorporation of robustness measures into optimisation processes, which requires a significantly larger number of design evaluations [40].

There are different approaches to incorporating robustness measures into optimisation processes. For example, surrogate-assisted robust optimization methods. In [41], a strategy is proposed to enhance the local generalization capability of the surrogate model by incorporating sampling points near the Pareto front. The key idea is to focus on adding points that are adjacent to the Pareto front obtained from each optimization cycle, thus avoiding the dominated region. At the same time, the Polynomial Chaos Expansions method is employed to determine the probability distribution and the sensitivity of each design variable. An improved sequential Taguchi method that enhances the conventional approach by using a hierarchical optimization strategy for multi-objective optimization could result in a torque ripple error reduction from 5.57 % to 1.61 % in an axial-radial flux hybrid excitation permanent magnet synchronous motor [42]. After determining the sensitive parameters, the non-sensitive parameters are optimised first, followed by the rest. Introducing an uncertainty vector in the position of the control points that define the shape of the machine's air gap to an isogeometric formulation of an electric machine could increase the duration of the simulations by four times but reduce the torque ripple by 10 % [43].

This paper covers the former subcategory, which focuses on the analysis of a single optimum design with the prospect that the results obtained can be incorporated into the optimisation process later on. One of the uncertainties from an engineering point of view is the manufacturing tolerances covering erroneous shapes, like flux barrier width and erroneous positioning, for example, the positioning of the magnets [40] on which this paper focuses.

Another method proposed for robust design analysis and to reduce its computational burden is the worst-uncertain-combination-analysis (WUCA) method [44], which was implemented to estimate the worst-case torque ripple [45] or cogging torque [46] under manufacturing uncertainties for a PMSM. Also, a PM assembling approach was proposed to reduce the impact of PM uncertainties on cogging torque. This approach involves arranging the PMs with a specific offset one by one so that their effects can offset each other [47]. It is also possible to approach the problem from a statistical probability side [39] or using design-of-experiments methods [48].

The optimisation process with NSGA-II is deterministic as the parameters' variations are not considered; however, there are many unavoidable manufacturing uncertainties such as manufacturing tolerances, assembly accuracy and material tolerances [38]. Based on

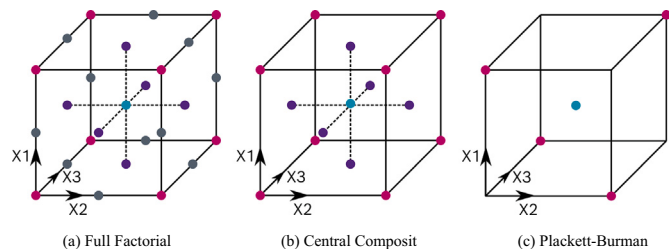


Fig. 11. Representation of the design space with three factors as design variables and three levels is represented as a cube [49].

[48], the design of experiment methods, for example, the Central Composite (CC) design-based sampling, can approximate the extrema precisely while reducing the number of models to calculate by approximately 96 %. The Plackett–Burman (PB) sampling method reduces the design space by more than 99 % with a 20 % approximation error. The samplings of the DOE methods are illustrated in Fig. 11.

In this paper, the effects of the PM and MFB shifting and width are emphasised, meaning the manufacturing tolerances of the MFB and the assembling accuracy of the PM are approximated. The factors could be the width of PM (X_8) and the shift of PM (X_9) focusing on Cases A1 and A2, where the dimensions of the MFB are equal to the PM. In terms of Cases B1 and B2, the investigated design variables could be the width of PM (X_8), the width of MFB (X_9), the shifting angle of PM (X_{10}) and the shifting angle of MFB (X_{11}) depending on which case is optimal. The established tolerances are ± 0.15 degrees at maximum, which means approximately ± 0.06 mm displacement at each design variable. For each design variable it introduces a discrete uncertainty of -0.06 mm, 0 mm or $+0.06$ mm. As it is possible to use the Taguchi method not only to do sensitivity analysis but to approximate the extrema so robust design analysis [50], an L25 orthogonal array was used for the sampling of the Full Factorial design space because it offers less simulations than the Central Composite method and expected to approximate the extrema better than the Plackett–Burman method. The investigated machine is robust if the difference between the extrema and the optimal value is lower than a predetermined threshold unique to every machine and use case. In this paper, this threshold is defined at 5 %. The full factorial is also calculated to validate the Taguchi method's approximation.

3. Results

3.1. Sensitivity analysis

The sensitivity analysis results with the Taguchi method are shown in Figs. 12 and 13 where a higher SSB value corresponds to higher sensitivity of the objectives to the given design variables. As this paper focuses on PM and MFB shifting, the parameters X_8 and X_9 are in scope for Cases A1 and A2. Similarly X_8 , X_9 , X_{10} and X_{11} are investigated in Cases B1 and B2. The cumulated comparison is possible due to the normalisation step in the sensitivity analysis. Both Figs. 12 and 13 show that the parameters related to PM and MFB shifting have a negligible effect on the average torque output compared to the cogging torque and torque ripple in line with [21,22]. Thus, emphasis will be placed on the latter two objectives. Regarding cogging torque and torque ripple, the parameter X_7 —which corresponds to the height of the magnet similar to the magnet used in [14]—has a significant distortion effect. To highlight the effect on PM and MFB shifting parameters later in Section 3.3, the parameter X_7 is fixed at 1.5 millimetres. The PM might be thin but is manufacturable according to [14] and our local manufacturer partner, too. The average torque is highly sensitive to the change of the X_1 parameter, which is the opening angle of the CFB. The equivalent magnetic circuit model of the FI-PMASynRM is defined in [19]. It also defines the equivalent magnetic circuit of flux barriers on the magnetic flux path of the q-axis where the following Eq. (4) obtains the CFB reluctance (R_{CFB}).

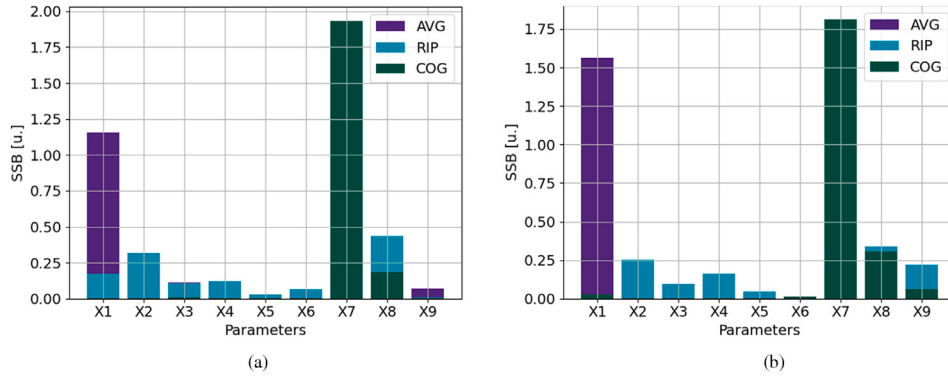


Fig. 12. Cumulated sensitivity of (a) Case A1 and (b) Case A2 where AVG: average torque, RIP: torque ripple and COG: cogging torque.

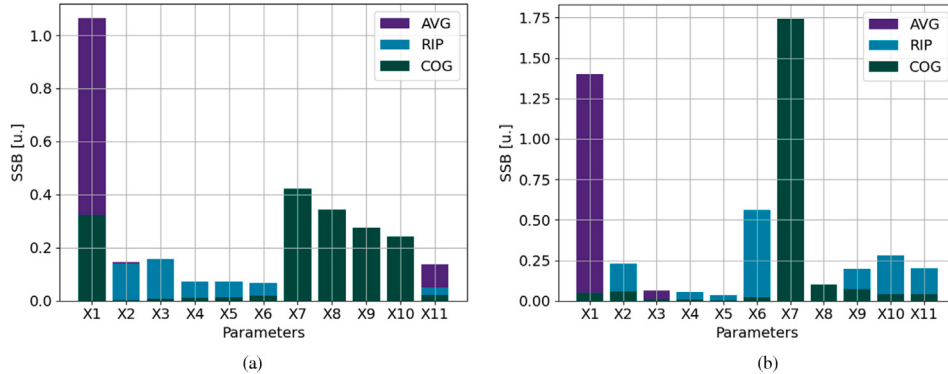


Fig. 13. Cumulated sensitivity of (a) Case B1 and (b) Case B2 where AVG: average torque, RIP: torque ripple and COG: cogging torque.

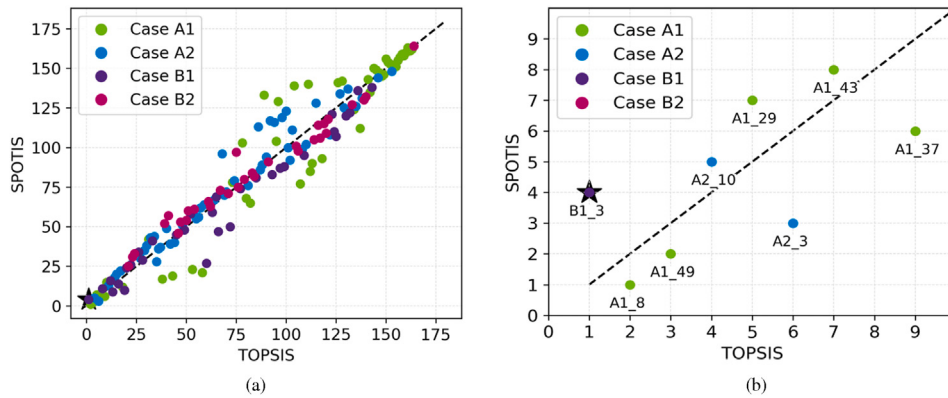


Fig. 14. (a) Ranking of all 164 unique models by TOPSIS and SPOTIS with entropy weights where the diagonal shows equal ranking between the two methods, (b) ranking of the first seven models.

$$R_{CFB} = \frac{l_{CFB}}{\mu_0 A_{CFB}} \quad (4)$$

where:

- l_{CFB} : depth of the cut-off barrier (proportional to X1 and X2)
- A_{CFB} : cross-sectional area of the cut-off barrier perpendicular to the flux direction (proportional to X1 and X2).

The X1 and X2 parameters together determine the depth and area of the cut-off barrier. The depth also increases the reluctance, corresponding to a lower inductance value. The X1 and X2 parameters are coupled in this geometric sense, which could explain the lack of

average torque sensitivity for the X2 parameter identified by the sensitivity analysis. In line with the torque Eq. (2) of the machine, the saliency ratio is increased by reducing the quadrature inductance, thus increasing the torque, which is the expected result.

3.2. Optimisation

The NSGA-II optimisation resulted in 164 different solutions out of the population of 50 for each four different cases, meaning that some models in the Pareto front from Cases B1 and B2 were similar to Cases A1 or A2 as there is a possibility where the width of the MFB and the PM are equal in Cases B1 and B2. This implies that the presence of air barriers

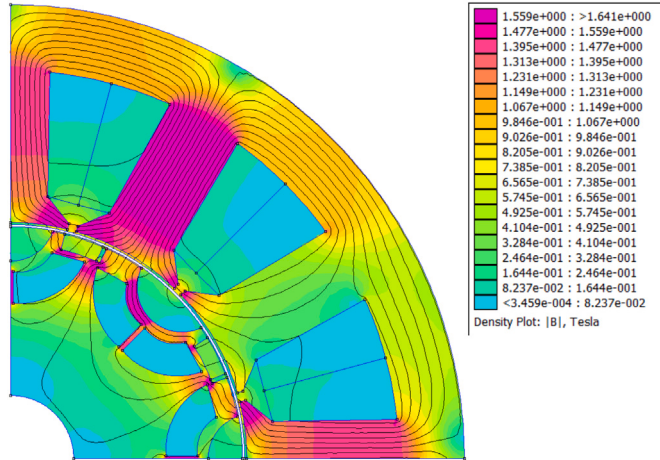


Fig. 15. The flux density map of the optimal design at maximal torque.

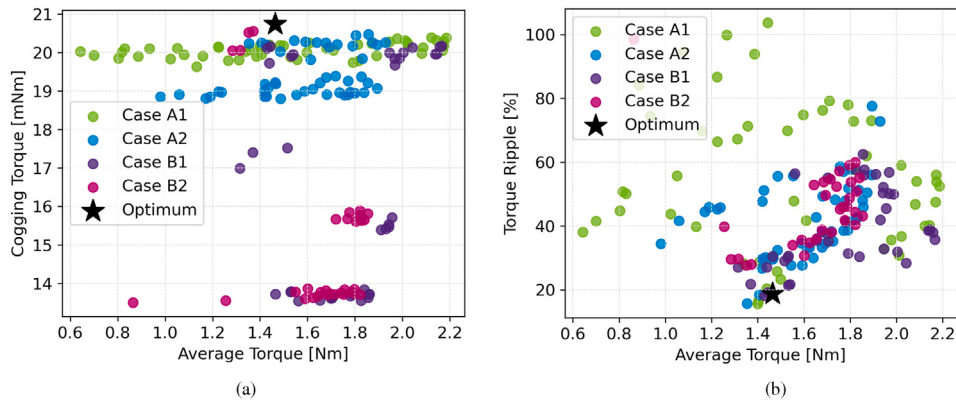


Fig. 16. Comparison of each model in the scope of the objectives (a) average torque to cogging torque and (b) torque ripple to cogging torque.

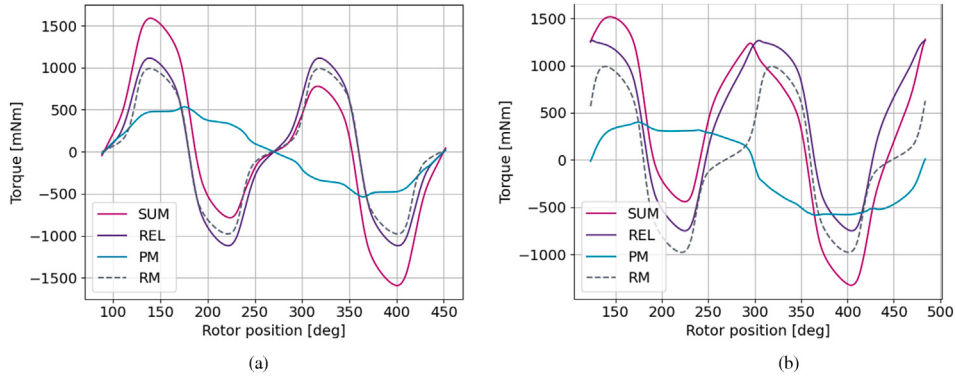


Fig. 17. Comparison of the torque components compared (a) an FI-PMASynRM model without shifting and (b) with the optimal FI-PMASynRM model with PM shifting and air barriers where the SUM is the complete torque of the machine, REL is the reluctance component, PM is the magnetic component, and RM is the baseline reluctance component calculated without PM and MFB.

next to the magnet could result in a better design than in some cases without them, but not in all. Fig. 14a shows the ranking of all 164 unique models by TOPSIS and SPOTIS with entropy weights where the diagonal shows equal ranking between the two methods for all four cases. All the cases show an even distribution along the diagonal line by ranking, implying that all the cases could be equally good solutions as there is no clear separation between them. Fig. 14b presents the ranking of the first seven models where the only model from Case B is *B1_3* ranked #1 by TOPSIS and #4 by SPOTIS, implying that the given circumstances might

favour Case A. However, as *B1_3* ranked high and this paper focuses on shifting the MFB and PM by introducing air barriers, only present in Case B, the *B1_3* is chosen as an optimal design.

The flux density map of the optimal design at maximal torque is shown in Fig. 15. The value of the design variables of the optimal model are X_1 : 21 deg, X_2 : 140 deg, X_3 : 1 mm, X_4 : 0.5 mm, X_5 : 3 mm, X_6 : 1 mm, X_7 : 1.5 mm, X_8 : 10 deg, X_9 : 11 deg, X_{10} : 16 deg and X_{11} : 14 deg meaning a significant shifting counter-clockwise and the introduction of an air barrier on the right side of the magnets.

Table 5

Comparison of Taguchi and Full Factorial methods with the optimal values, where AVG: average torque, RIP: torque ripple, COG: cogging torque, MIN: minimum value, MEAN: mean value, MAX: maximum value and OPT: the results of the optimisation.

Metric	Method	MIN	MEAN	MAX	OPT
AVG (mNm)	Taguchi	1431.08	1449.11	1469.86	1463.40
	Full Factorial	1429.05	1450.11	1471.37	—
	Difference	2.03	-1.00	-1.51	—
RIP (%)	Taguchi	18.89	19.66	20.72	18.81
	Full Factorial	18.41	19.67	21.59	—
	Difference	0.48	-0.01	-0.87	—
COG (mNm)	Taguchi	20.45	20.73	21.01	20.74
	Full Factorial	20.41	20.74	21.11	—
	Difference	0.04	-0.01	-0.10	—

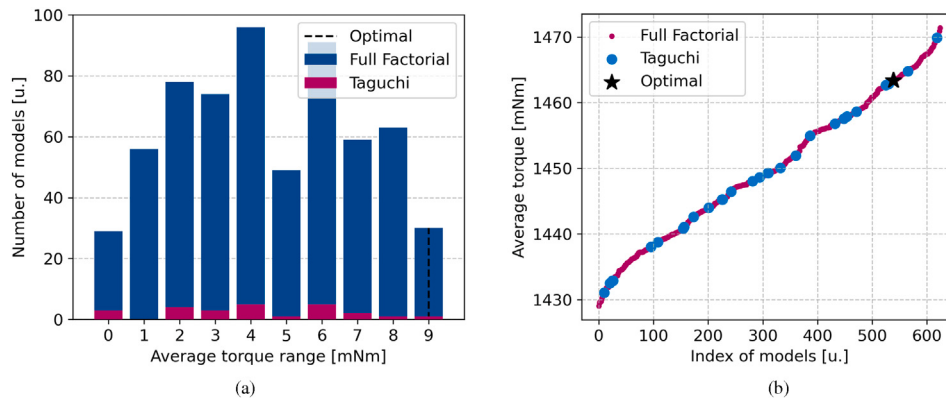


Fig. 18. The comparison of Taguchi and Full Factorial calculations for average torque (a) the number of models distributed in bins of $1429.05 + (1471.37 - 1429.05)/10 * i \in [0..9]$ and (b) the coverage of the Taguchi method for the Full Factorial calculations.

Fig. 16 represents the comparison of each model in the scope of the objectives case by case. With the introduction of PM shifting and air barriers, not only can the torque ripple be reduced in line with [21], but one can also significantly reduce the amplitude of the cogging torque, too, regardless of whether the magnets are shifted in one direction or opposite to each other, as seen in **Fig. 16a**. Regardless of the significant approx. 34 % possible cogging torque reduction, the optimal model fulfils the cogging torque requirements and was chosen by the average torque and torque ripple requirements. As shown in **Fig. 16b**, only a few models fulfil the torque ripple requirements of less than 20 %. The possible candidates are from Cases A1, A2 and B1.

Fig. 17 presents the comparison of the torque components. The dashed line in both figures represents the reluctance torque where the MFB and PM are absent as a baseline. In **Fig. 17a**. The torque components of the machine are shown without magnet shifting, which is in line with the analytical prediction of **Fig. 4b**. In **Fig. 17b**, the optimal machine's torque components are shown with MFB and PM shifting. In both cases, a 50 % torque surplus can be reached compared to the machine without MFB and PM. Still, in the case without MFB and PM shifting, a volume of 2848.35 mm³ PM is necessary to achieve approximately the same torque output, whereas with MFB and PM shifting, only a volume of 1958.27 mm³ PM is needed, meaning less PM mass. The MFB and PM shifting introduce an asymmetry to the machine, reducing the torque output of the reverse motorizing, but in micromobility applications such as e-scooters and e-bikes, the reverse motorizing application is rarely used. The forward motorizing condition meets the requirements.

3.3. Robust design analysis

Table 5 summarises the results of the Taguchi and Full Factorial methods compared to each other and to the optimal machine. The comparison of the Taguchi and Full Factorial methods validates how well the

Taguchi method approximates the extrema with fewer simulations compared to all the possibilities. It is shown that the differences are less than 1 % in each case, meaning the Taguchi method is an effective sampling method in this particular case as well. In terms of robustness compared to the optimal case, the average torque varies in the range of [-34.35 mNm, +7.97 mNm], which is a 2.35 % change that is within the initial 5 % threshold and still higher than the 1400 mNm requirement. In the case of the torque ripple, the range is in [-0.40 %, +2.78 %], which is a 14.77 % change in terms of robustness outside the initial 5 % threshold, and there is a possibility that it exceeds the 20 % requirement. The cogging torque is in the range of [-0.33 mNm, +0.37 mNm], which is a 1.79 % change still within the initial 5 % threshold and 22 mNm requirement. The results show that the machine is expected to be robust in terms of average torque and cogging torque. Still, the width and the shift of MFB and PM can significantly change the torque ripple even within the manufacturing tolerance range.

In **Fig. 18a**, the comparison of Taguchi and Full Factorial calculations for average torque is shown where the number of models is distributed in bins of $1429.05 + (1471.37 - 1429.05)/10 * i \in [0..9]$. The figure represents how likely the manufactured machine falls in a range of average torque, assuming the higher number of models is proportional to the probability. The manufactured machine will likely have a lower torque than the optimal value.

Fig. 18b shows the sorted results of all models, which is an evenly distributed linear probability without any outliers, extremes or gaps, indicating less sensitivity and robustness. It can also be seen that the Taguchi method evenly samples the whole design space. **Fig. 19a** shows the comparison of Taguchi and Full Factorial calculations for torque ripple with the number of models distributed in bins of $18.41 + (21.59 - 18.41)/10 * i \in [0..9]$. The bin #5 range is still under the initial 20 % requirement, and if the number of models is proportional to the probability of the manufacturing outcome, it is only 12.10 % likely that the machine falls in a range higher than bin #5, meaning outside of the torque

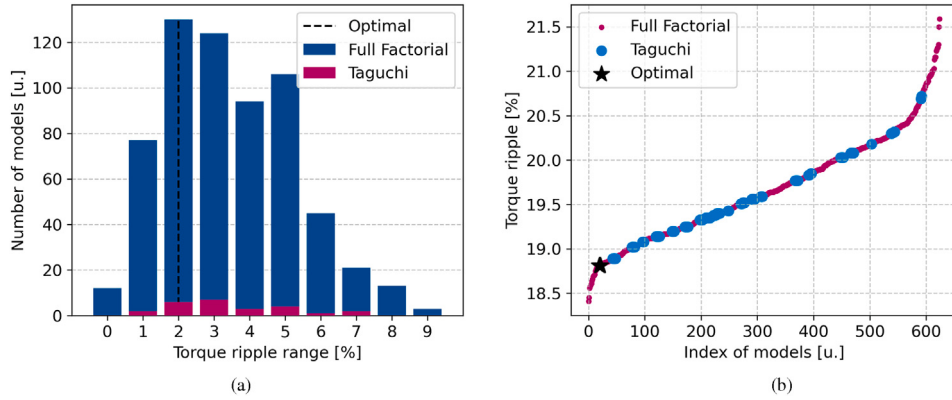


Fig. 19. The comparison of Taguchi and Full Factorial calculations for torque ripple (a) the number of models distributed in bins of $18.41 + (21.59 - 18.41)/10 * i \in [0..9]$ and (b) the coverage of the Taguchi method for the Full Factorial calculations.

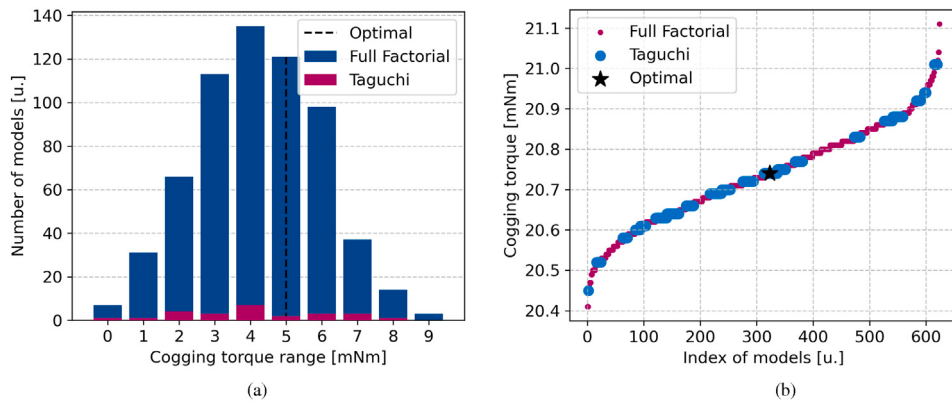


Fig. 20. The comparison of Taguchi and Full Factorial calculations for average torque (a) the number of models distributed in bins of $20.41 + (21.11 - 20.41)/10 * i \in [0..9]$ and (b) the coverage of the Taguchi method for the Full Factorial calculations.

ripple requirements. Nevertheless, there are some possible methods to further reduce the torque ripple, as skewing the rotor [51]—which also increases the manufacturing complexity—increasing the number of flux barriers [52] or injecting compensating currents through dq-axis modulation from control side [53,54]. Fig. 19b shows all the models sorted, and at the extremes, some models are present, which deviate from the even linear distribution corresponding to the numeric result presented in Table 5. Furthermore, the Taguchi method does not cover these extremes. Fig. 20a shows the comparison of Taguchi and Full Factorial calculations for average torque with the number of models distributed in bins of $20.41 + (21.11 - 20.41)/10 * i \in [0..9]$ meaning an even distribution and less likelihood of extremes. Fig. 20b shows a similar result to Fig. 19b but with higher coverage of the extremes by the Taguchi method.

Fig. 21 represents the sensitivity of each objective function for the change in the parameters corresponding to MFB and PM calculated on the Full Factorial results within the manufacturing tolerance ranges. It shows that X_8 , the width of the PM, affects the average torque the most, while the width of the MFB affects the torque ripple significantly in line with the results of [22]. The change within the manufacturing tolerance range of the shifting of both the PM and MFB is affecting the cogging torque higher than the other two design variables but not the average torque and the cogging torque. The X_{10} design variable, which is the shift of the PM, is the only parameter that corresponds to assembly and not precise manufacturing, like the width of the PM (X_8) and MFB (X_9) or the shift of MFB (X_{11}). The results imply that the machine is

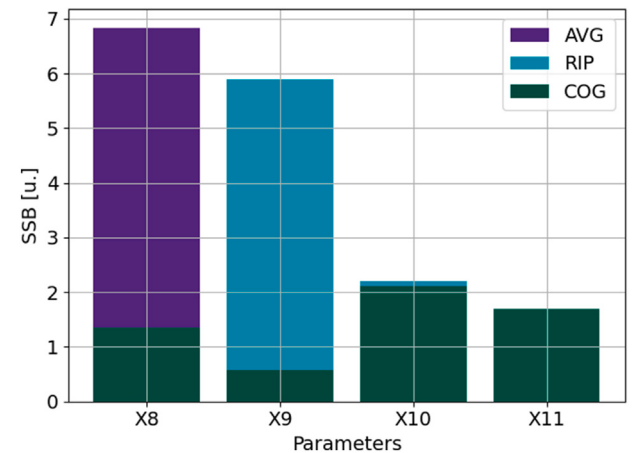


Fig. 21. The sensitivity of each parameter corresponding to MFB and PM using ANOVA for the Full Factorial results where AVG: average torque, RIP: torque ripple and COG: cogging torque.

less sensitive to the changes of the X_{10} parameter corresponding to the assembly, which is inherently a less precise manufacturing step than the laser cutting of the steel sheets, for example, meaning fewer machines that differ from the expected output in mass production.

4. Conclusion

This research covered the optimisation process and robustness analysis of a flux-intensifying permanent magnet-assisted synchronous reluctance machine focusing on the surface inset magnets. The inset magnets are placed in the rotor's circumference, simplifying the disassembly process and aiding in the reuse or recycling of the magnets and the machine at its end-of-life. The study assessed how rotor dimensions influence average torque, torque ripple, and cogging torque, including magnet shifting. These were analysed using the Taguchi method during sensitivity and robustness calculations, NSGA-II during the optimisation, and SPOTIS and TOPSIS methods during multi-criteria decision-making. The findings indicate that by implementing permanent magnet shifting and air barriers, not only was the torque ripple reduced, but the cogging torque amplitude could also be decreased. The NSGA-II optimisation highlighted that having air barriers adjacent to the magnets could lead to a superior design compared to cases without these barriers, although this is not universally applicable. However, regarding the optimal machine topology, 31.2 % less magnet volume is required to produce a similar torque output with shifting and air barriers than without those, resulting in a reduced permanent magnet mass. The shifting does introduce asymmetry to the machine, which could decrease torque output during reverse motoring. However, reverse motoring is infrequently used in micromobility applications like e-scooters and e-bikes. The machine presents robustness concerning average and cogging torque; however, the width and shift of both the magnet flux barrier and permanent magnet can considerably alter the torque ripple, even within acceptable manufacturing tolerances. A comparison of the Taguchi and Full Factorial methods confirmed the Taguchi method's ability to identify extrema with fewer simulations in this particular case. Due to manufacturing tolerance variations, torque ripple can exceed the pre-defined requirements; however, the likelihood of this outcome during manufacturing is only 12.10 %. The shift of the permanent magnet is the only parameter linked to assembly rather than precise manufacturing, unlike the width of the permanent magnet and magnet flux barrier or the shift of the magnet flux barrier. The results suggest that the machine has less sensitivity to changes in the shift of the permanent magnet related to assembly, which is inherently a less accurate manufacturing process than the laser cutting of the steel sheets, indicating fewer machines will differ from expected manufacturing outputs during mass production. This study's findings support the premise that the redesigned machine's torque output, torque ripple, and cogging torque are affected more by the variations in the primary geometrical parameters of the rotor within manufacturing tolerances than by the positioning of the shifted magnets. This research is part of a broader investigation aimed at remanufacturing an existing electrical machine with a 3D printed FIPMaSynRM rotor utilising surface-inset ferrite magnets; the following step will be manufacturing and measuring, thus validating the results.

CRediT authorship contribution statement

Mihály Katona: Writing – original draft, Visualization, Validation, Software, Methodology, Investigation, Funding acquisition, Data curation, Conceptualization. **Tamás Orosz:** Writing – review & editing, Writing – original draft, Supervision, Software, Methodology, Funding acquisition, Conceptualization.

Funding

Project No. 147030 was implemented with support provided by the National Research, Development, and Innovation Fund of Hungary, financed under the FK funding scheme. Project No. 2023-2.1.2-KDP-2023-00017 has been implemented with the support provided by the Ministry of Culture and Innovation of Hungary from the National Research, Development and Innovation Fund, financed under the KDP-2023 funding scheme.

Declaration of competing interest

The authors declare the following financial interests/personal relationships which may be considered as potential competing interests:

Mihály Katona reports that financial support was provided by Ministry of Culture and Innovation of Hungary. Tamás Orosz reports that financial support was provided by Ministry of Culture and Innovation of Hungary. If there are other authors, they declare that they have no known competing financial interests or personal relationships that could have appeared to influence the work reported in this paper.

Data availability

The authors have shared their code at <https://github.com/tamasorosz/py2femm/tree/synrm>.

References

- [1] Katona M, Orosz T. Circular economy aspects of permanent magnet synchronous reluctance machine design for electric vehicle applications: a review. Energies 2024;17(6). <https://doi.org/10.3390/en17061408>
- [2] Schlesinger L, Koller J, Oechsle O, Molenda P. Remanufacturing of E-mobility components - five-step implementation strategy to increase sustainability within circular economy. In: 2021 11th international electric drives production conference (EDPC); 2021. p. 1–8. <https://doi.org/10.1109/EDPC53547.2021.9684200>
- [3] Gharalkar M, Ali Z, Hillier G. Clarifying the disagreements on various reuse options: repair, recondition, refurbish and remanufacture. Waste Manag Res 2016;34(10):995–1005. <https://doi.org/10.1177/0734242X16628981>
- [4] Kirchherr J, Reike D, Hekkert M. Conceptualizing the circular economy: an analysis of 114 definitions. Resour Conserv Recycl 2017;127:221–32. <https://doi.org/10.1016/j.resconrec.2017.09.005>
- [5] Li Z, Wang P, Che S, Du S, Li Y, Sun H. Recycling and remanufacturing technology analysis of permanent magnet synchronous motor. Clean Technol Environ Policy 2022;24(6):1727–40. <https://doi.org/10.1007/s10098-022-02279-0>
- [6] Li Z, Che S, Wang P, Du S, Zhao Y, Sun H, et al. Implementation and analysis of remanufacturing large-scale asynchronous motor to permanent magnet motor under circular economy conditions. J Clean Prod 2021;294:126233. <https://doi.org/10.1016/j.jclepro.2021.126233>
- [7] Liu M, Chen L, Sheng X, Yang Y, Yu F, Li Y, et al. Dynamic simulation of life cycle environmental benefits of remanufacturing asynchronous motors to permanent magnet synchronous motors. J Clean Prod 2023;426:138932. <https://doi.org/10.1016/j.jclepro.2023.138932>
- [8] Katona M, Bánya DG, Németh Z, Kuczmann M, Orosz T. Remanufacturing a synchronous reluctance machine with aluminum winding: an open benchmark problem for FEM analysis. Electronics 2024;13(4). <https://doi.org/10.3390/electronics13040727>
- [9] Tiwari D, Misra J, Tiwari A, Jewell GW. A review of circular economy research for electric motors and the role of industry 4.0 technologies. Sustainability 2021;13(17). <https://doi.org/10.3390/su13179668>
- [10] Li Z, Hamidi AS, Yan Z, Sattar A, Hazra S, Soulard J, et al. A circular economy approach for recycling electric motors in the end-of-life vehicles: a literature review. Resour Conserv Recycl 2024;205:107582. <https://doi.org/10.1016/j.resconrec.2024.107582>
- [11] Casper R, Sundin E. Electrification in the automotive industry: effects in remanufacturing. J Remanuf 2021;11(2):121–36. <https://doi.org/10.1007/s13243-020-00094-8>
- [12] European Parliament, Council of the European Union. Directive 2000/53/EC of the European Parliament and of the Council of 18 September 2000 on end-of-life vehicles - commission statements. Official Journal of the European Union, cELEX:32000L0053; 2000.
- [13] Kocsis B, Windisch M, Mészáros I, Károly Varga L. 3D printing parameters optimization for Fe-6.5 wt%Si. J Magn Magn Mater 2024;592:171829. <https://doi.org/10.1016/j.jmmm.2024.171829>
- [14] Ngo D-K, Hsieh M-F, Huynh TA. Torque enhancement for a novel flux intensifying PMA-SynRM using surface-inset permanent magnet. IEEE Trans Magn 2019;55(7):1–8. <https://doi.org/10.1109/TMAG.2019.2897022>
- [15] Huynh TA, Hsieh M-F, Shih K-J, Kuo H-F. Design and analysis of permanent-magnet assisted synchronous reluctance motor. In: 2017 20th international conference on electrical machines and systems (ICEMS); 2017. p. 1–6. <https://doi.org/10.1109/ICEMS.2017.8056462>
- [16] Briggner V. Design and comparison of PMaSynRM versus PMSM for pumping applications, id: diva2: 1249540 [Accessed 29 May 2018].
- [17] Hsieh M-F, Ngo D-K, Thao NGM. Flux intensifying feature of permanent magnet assisted synchronous reluctance motor with high torque density. Electronics 2022;11(3). <https://doi.org/10.3390/electronics11030397>
- [18] Ngo D-K, Hsieh M-F, Dung Le T. Analysis on field weakening of flux intensifying synchronous motor considering PM dimension and armature current. IEEE Trans Magn 2021;57(2):1–5. <https://doi.org/10.1109/TMAG.2020.3023176>
- [19] Hsieh M-F, Ngo D-K, Do V-V, Wu C-H, Wu YK. Inductance calculation of flux intensifying PMa-SynRM by equivalent magnetic circuit. In: 2022 7th national scientific conference on applying new technology in green buildings (ATiGB); 2022. p. 135–40. <https://doi.org/10.1109/ATiGB56486.2022.9984074>

- [20] Wellmann T, Tousignant T, Govindswamy K, Tomazic D, Steffens C, Janssen P. NVH aspects of electric drive unit development and vehicle integration. Technical Report 2019-01-1454. SAE International; 2019. <https://doi.org/10.4271/2019-01-1454>
- [21] Liu G, Du X, Zhao W, Chen Q. Reduction of torque ripple in inset permanent magnet synchronous motor by magnets shifting. *IEEE Trans Magn* 2017;53(2):1–13. <https://doi.org/10.1109/TMAG.2016.2620422>
- [22] Du X, Liu G, Chen Q, Xu G, Xu M, Fan X. Optimal design of an inset PM motor with assisted barriers and magnet shifting for improvement of torque characteristics. *IEEE Trans Magn* 2017;53(11):1–4. <https://doi.org/10.1109/TMAG.2017.2699684>
- [23] Nagarajan VS, Kamaraj V, Sivaramakrishnan S. Geometrical sensitivity analysis based on design optimization and multiphysics analysis of PM assisted synchronous reluctance motor. *Bull Pol Acad Sci Tech Sci* 2019;67(1):155–63. <https://doi.org/10.24425/bpas.2019.127345>
- [24] Andriushchenko E, Kallaste A, Mohammadi MH, Lowther DA, Heidari H. Sensitivity analysis for multi-objective optimization of switched reluctance motors. *Machines* 2022;10(7). <https://doi.org/10.3390/machines10070559>
- [25] Fraley S, Zalewski J, Oom M, Terrien B. Chemical process dynamics and controls. In: Ch. Design of experiments via Taguchi methods - orthogonal arrays. he LibreTexts; 2024. p. 14.1.1–14.1.10.
- [26] Voice A, Wilkins A, Parambi R, Oraiqat I. Chemical process dynamics and controls. In: Ch. Factor analysis and ANOVA. he LibreTexts; 2024. p. 13.12.1–13.12.14.
- [27] Hua Y, Zhu H, Gao M, Ji Z. Multiobjective optimization design of permanent magnet assisted bearingless synchronous reluctance motor using NSGA-II. *IEEE Trans Ind Electron* 2021;68(11):10477–87. <https://doi.org/10.1109/TIE.2020.3037873>
- [28] Xu H, Li J. Automatic design optimization of a permanent magnet assisted synchronous reluctance motor with field line shaped barriers. In: 22nd international conference on the computation of electromagnetic fields (COMPUMAG); 2019. <https://api.semanticscholar.org/CorpusID:247289929>
- [29] Xu G, Jia Z, Chen Q, Xia J, Cai Y, Zhang Z. A fast and effective optimization procedure for the ferrite PMASyRM to reduce material cost. *IEEE Trans Transp Electrif* 2024;10(1):635–47. <https://doi.org/10.1109/TTE.2023.3291489>
- [30] Blank J, Deb K. Pymoo: multi-objective optimization in Python. *IEEE Access* 2020;8:89497–509.
- [31] Orosz T. p2femm. 2024. <https://github.com/tamasorosz/py2femm> [Accessed 25/11/2024].
- [32] Meeker D. FEMM 4.2 - finite element method magnetics. 2020. <https://www.femm.info/wiki/HomePage> [Accessed 25/01/2024].
- [33] Son J-C, Lim D-K. Novel stator core of the permanent magnet assisted synchronous reluctance motor for electric bicycle traction motor using grain-oriented electrical steel. In: 2021 24th international conference on electrical machines and systems (ICEMS); 2021. p. 1215–18. <https://doi.org/10.23919/ICEMS52562.2021.9634439>
- [34] Salehinia SR, Afjei SE, Hekmati S. Analytical method for optimal design of synchronous reluctance motor for electric scooter application. *Sci Iran* 29 (5) (2022) 2537–2551. <https://doi.org/10.24200/sci.2021.56496.4748>.
- [35] Naseh M, Hasanzadeh S, Dehghan SM, Rezaei H, Al-Sumaiti AS. Optimized design of rotor barriers in PM-assisted synchronous reluctance machines with Taguchi method. *IEEE Access* 2022;10:38165–73. <https://doi.org/10.1109/ACCESS.2022.3165549>
- [36] Dezert J, Tchamova A, Han D, Tacnet J-M. The SPOTIS rank reversal free method for multi-criteria decision-making support. In: 2020 IEEE 23rd international conference on information fusion (FUSION); 2020. p. 1–8. <https://doi.org/10.23919/FUSION45008.2020.9190347>
- [37] Chen P. Effects of the entropy weight on topsis. *Expert Syst Appl* 2021;168:114186. <https://doi.org/10.1016/j.eswa.2020.114186>
- [38] Lei G, Zhu J, Guo Y, Liu C, Ma B. A review of design optimization methods for electrical machines. *Energies* 2017;10(12). <https://doi.org/10.3390/en10121962>
- [39] Credo A, Fabri G, Villani M, Popescu M. A robust design methodology for synchronous reluctance motors. *IEEE Trans Energy Convers* 2020;35(4):2095–105. <https://doi.org/10.1109/TEC.2020.3016567>
- [40] Bramerdorfer G, Marth E. Tolerance analysis and robust optimization for electric machine design. In: IKMT 2022; 13. GMM/ETG-Symposium; 2022. p. 1–7.
- [41] Liu L, Ma Y, Wang R, Li Z, Sun L, Zhao H. Robust optimization of a stator tooth chamfering IPMSM for electric power steering applications. In: 2024 international conference on electrical machines (ICEM); 2024. p. 1–7. <https://doi.org/10.1109/ICEM60801.2024.10700320>
- [42] Xu N, Li N, Sun X, Wang Y, Wan B. Robust multi-objective optimisation of an axial-radial flux hybrid excitation permanent magnet synchronous motors based on improved sequential Taguchi method. *IET Electr Power Appl* 2025;19(1):e12543. <https://doi.org/10.1049/elp2.12543>
- [43] Komann T, Wiesheu M, Ulbrich S, Schöps S. Robust design optimization of electric machines with isogeometric analysis. *Mathematics* 2024;12(9). <https://doi.org/10.3390/math12091299>
- [44] Yang Y, Bianchi N, Zhang C, Zhu X, Liu H, Zhang S. A method for evaluating the worst-case cogging torque under manufacturing uncertainties. *IEEE Trans Energy Convers* 2020;35(4):1837–48. <https://doi.org/10.1109/TEC.2020.2996098>
- [45] Yang Y, Bianchi N, Bramerdorfer G, Kong Y, Zhang C, Zhang S. A method to estimate the worst-case torque ripple under manufacturing uncertainties for permanent magnet synchronous machines. In: 2020 IEEE energy conversion congress and exposition (ECCE); 2020. p. 4075–82. <https://doi.org/10.1109/ECCE44975.2020.9236291>
- [46] Yang Y, Bianchi N, Bramerdorfer G, Zhang C, Zhang S. Methods to improve the cogging torque robustness under manufacturing tolerances for the permanent magnet synchronous machine. *IEEE Trans Energy Convers* 2021;36(3):2152–62. <https://doi.org/10.1109/TEC.2020.3048051>
- [47] Liu H, Jin X, Bianchi N, Bramerdorfer G, Hu P, Zhang C, et al. A permanent magnet assembling approach to mitigate the cogging torque for permanent magnet machines considering manufacturing uncertainties. *Energies* 2022;15(6). <https://doi.org/10.3390/en15062154>
- [48] Katona M, Kuczmann M, Orosz T. Accuracy of the robust design analysis for the flux barrier modelling of an interior permanent magnet synchronous motor. *J Comput Appl Math* 2023;429:115228. <https://doi.org/10.1016/j.cam.2023.115228>
- [49] Orosz T, Gádó K, Katona M, Rassölkín A. Automatic tolerance analysis of permanent magnet machines with encapsulated fem models using digital-twin-distiller. *Processes* 2021;9(11). <https://doi.org/10.3390/pr9112077>
- [50] Lee S, Kim K, Cho S, Jang J, Lee T, Hong J. Optimal design of interior permanent magnet synchronous motor considering the manufacturing tolerances using Taguchi robust design. *IET Electr Power Appl* 2014;8(1):23–28. <https://doi.org/10.1049/iet-epa.2013.0109>
- [51] Hubert T, Reinlein M, Kremser A, Herzog H-G. Torque ripple minimization of reluctance synchronous machines by continuous and discrete rotor skewing. In: 2015 5th international electric drives production conference (EDPC); 2015. p. 1–7. <https://doi.org/10.1109/EDPC.2015.7323229>
- [52] Zhequan W, Dejun Y, Lujun C, Jia F. Design of magnetic barrier angle of permanent magnet assisted synchronous reluctance motor based on minimum torque ripple. In: 2022 7th Asia conference on power and electrical engineering (ACPEE); 2022. p. 1712–16. <https://doi.org/10.1109/ACPEE53904.2022.9783897>
- [53] Qu J, Zhang P, Jatskevich J, Zhang C. Torque-ripple reduction of permanent magnet synchronous machine drives based on novel speed harmonic control at low-speed operation. *IEEE Trans Ind Electron* 2023;70(8):7683–94. <https://doi.org/10.1109/TIE.2022.3229379>
- [54] Qu J, Li X, Gao F, Zhang C, Zhang P. Torque ripple reduction of permanent magnet synchronous machine drives with tangential vibration acceleration control. *IEEE Trans Power Electron* 2025;40(4):4902–13. <https://doi.org/10.1109/TPEL.2024.3510430>

Glossary

- EoL*: end-of-life
PMSM: permanent magnet synchronous machine
REE: rare earth elements
PM: permanent magnet
FI-PMASyRM: flux-intensifying permanent magnet-assisted synchronous reluctance machine
PMASyRM: permanent magnet-assisted synchronous reluctance machine
MFB: magnet flux barrier
IFB: interior flux barrier
CFB: cut-off flux barrier
FI-IPM: flux-intensifying interior permanent magnet synchronous machine
SyRM: synchronous reluctance machine
FB: flux barrier
inset SPMSM: surface-mounted permanent magnet synchronous motor with inset magnets
RU: repeating units
ANOVA: analysis of variance
SSG: sum of squares between groups
NSGA II: non-dominated sorting genetic algorithm II
TOPSIS: the order preference by similarity to an ideal solution
SPOTIS: stable preference ordering towards ideal solution
WUCU: worst-uncertain-combination-analysis